Supporting Information

Fe-N-C/Fe nanoparticle composite catalysts for oxygen reduction reaction in proton exchange membrane fuel cells

Shiyang Liu, Quentin Meyer, Yibing Li, Tingwen Zhao, Zhen Su, Karin Ching, and Chuan Zhao*

School of Chemistry, The University of New South Wales, Sydney, New South Wales 2052, Australia

* Corresponding author. E-mail: chuan.zhao@unsw.edu.au

SI Table of Contents

1. Experimental section 1

2. Supplemental Figures 4

3. Supplemental Tables 11

4. References 13

1. Experimental section

1.1 Catalyst synthesis

Preparation of ZIF-8 and N-C host: ZIF-8 NPs were prepared following a reported method with minor modification [1]. In a typical procedure, 2.94 g Zn $(NO_3)_2 \cdot 6H_2O$ was dissolved in 100 mL methanol, 3.24g 2-methylimidazole 2MIm was dissolved in another 100 mL methanol. Then, two solution was mixed and stirred for 2.5 h under room temperature. The white sediments were centrifuged and washed with methanol for three times and then dried overnight at 60 °C in vacuum. N-C-host was obtained by pyrolyzing ZIF-8 in a tube furnace at 1000 °C in N_2 or Ar for 1 h.

Preparation of Fe-N-C-100/300/500 and N-C catalyst: Typically, 30 mg N-C-host was dissolved in 20 mL deionized water, followed by 1 h ultrasonic treatment to form a homogeneous suspension, then 100 μL $FeCl_3 \cdot 6H_2O$ solution (0.1 M) was added to the N-C-host solution and the resulting solution was stirred for another hour. The mixture was heated in an oil bath at 70 °C under stirring for 2 h, the resulting solution was directly dried at 200 °C, and the Fe^{3+} doped NC-host power was collected. The Fe-N-C-100 was obtained by heating the Fe^{3+} doped N-C-host power at 1000 °C under N_2 or Ar for 2 h. Fe-N-C-300/500 were prepared following a similar procedure using 300 and 500 μL of 0.1 M $FeCl_3 \cdot 6H_2O$ solution, respectively. N-C was prepared following the same procedure but without Fe doping.

1.2 Physical Characterizations

Transmission electron microscopy (TEM) accompanied by high-resolution transmission electron microscopy (HRTEM) was used to study the catalysts (JEOL F200). The high-angle annular dark-field (HAADF) was conducted on an FEI Themis-Z image, probe-corrected, and monochromated 60-300 kV STEM (Thermo Fisher, US). X-ray diffraction (XRD) was applied to analyze the crystal structures (Aeris, PANalytical). X-ray photoelectron spectroscopy (XPS) were applied to investigate the chemical compositions (Thermo ESCALAB250i). Inductively coupled plasma optical emission spectrometry (ICP-OES) was used to identify the Fe content in the catalysts (7300 PerkinElmer). Brunauer-Emmett-Teller (BET) surface areas were obtained using Tristar II 3020 instrument.

1.3 Rotating ring disk electrode (RRDE) measurements:

All half-cell testing were performed using a rotating ring disk electrode (RRDE, Pine Research Instrumentation, USA) with an electrochemical workstation (CHI 900B, CH Instruments) in 0.5M H_2SO_4 electrolyte. A glassy carbon disk (φ = 5mm) coated with

the catalyst ink was used as the working electrode. The reference electrode was a calibrated mercury-mercurous sulfate electrode, and a graphite rod was served as the counter electrode. All potentials reported in this work were calibrated to the reversible hydrogen electrode (RHE). Catalyst ink was prepared by dispersing 10 mg of catalyst in a solution of 0.885 mL isopropanol, 0.885 mL deionized water, and 0.230 mL Nafion alcohol solution (5 wt.%, Aldrich), followed by 1 h sonication. The Pt/C (20 wt.%) ink was made following a similar procedure. Catalyst loading is 600 μg cm^{-2} for N-C/Fe-N-C catalysts and 60 μg $_{Pt}$ cm^{-2} for Pt/C catalysts. All experiments were conducted at room temperature. The electrolyte was purged by O_2/Ar for 0.5 h before the tests. The RRDE tests were measured at different rotating speeds (400 to 1600 rpm). The oxygen reduction currents were obtained by subtracting the backgrounds currents measured in Ar-saturated electrolyte from the linear sweep voltammetry (LSV) measured in the O_2-saturated electrolyte. The stability of the catalysts was tested in the O_2-saturated 0.5 M H_2SO_4 electrolyte by applying a constant voltage at 0.5 V *vs*. RHE under a rotation speed of 200 rpm, data was recorded after stabilization. Methanol tolerance experiment was conducted by adding methanol into electrolyte during the i-t test at 0.5 V.

The peroxide yield (H_2O_2%) were calculated from the ring current (I_r) and the disk current (I_d) using equation 1:

$$H_2O_2\% = \frac{200\, I_r}{N|I_d|+I_r} \quad (1)$$

Where the current collection efficiency of the Pt ring (N) is 25%

The electron transfer number (*n*) was calculated by the equation 2:

$$n = \frac{4|I_d|}{|I_d|+I_r/N} \quad (2)$$

The Koutechky-Levich (K-L) plots are obtained by measuring the LSV curves at different rotation rates. The electron transfer number *n* can be calculated using the K-L equations:

$$\frac{1}{I} = \frac{1}{I_k} + \frac{1}{I_l} = \frac{1}{I_k} + \frac{1}{B\omega^{1/2}} \quad (3)$$

$$B=0.62nFC_0D_0^{2/3}\nu^{-1/6} \quad (4)$$

Where ω (rad s^{-1}) is the rotating rates of the RRDE (rad s^{-1}), I is the measured current density, I_k stands for the kinetic current density, and I_L is the limiting current

density. *n* represents the electron transfer number. F is the Faraday constant. *v* is the kinematic viscosity of the 0.5M H_2SO_4 (0.01009 $cm^2\ s^{-1}$). Dissolved oxygen concentration (C_0) equals 1.2×10^{-6} mol cm^{-3}. Diffusion coefficient of oxygen in the electrolyte (D_0) is $1.9 \times 10^{-5}\ cm^2\ s^{-1}$.

1.4 PEMFC tests

The ink mentioned above was also used to prepare the gas diffusion electrode (GDE). First, the ink was sonicated for 1h and stirred to form a homogeneous solution. Then the ink was drop casted on a piece of 1×1 cm^2 commercial gas diffusion layer (SGL29BC, Sigracet) on a hot plate (120 °C) and dried for 30 min. The loading for N/C and Fe-N-C was 3mg cm^{-2}. A control GDE of Pt/C (20 wt%) was prepared similarly with a 0.2 mg $_{pt}$ cm^{-2} loading. The commercial GDE (Fuel cell store, US) with a 0.2 mg $_{pt}$ cm^{-2} loading was used as the anode for all membrane electrode assemblies (MEAs). Nafion 211 membrane (fuel cell store, US) was sandwiched between the anode and as-prepared cathode, followed by hot-pressing at 130 °C for 90 s under 0.1 MPa to obtain the MEA. The MEA performance was measured by a commercial fuel cell test machine (850e, Scribner Associates Inc) with H_2 and O_2/Air with 100% relative humidity at 80 °C. The flow rate was 0.1 L min^{-1} for H_2 and 0.4 L min^{-1} for O_2/Air, respectively. The stability of catalyst was evaluated by holding the voltage of the fuel cell at 0.5 V for 50 hours with H_2 and air at ambient pressure.

2. Supplemental Figures

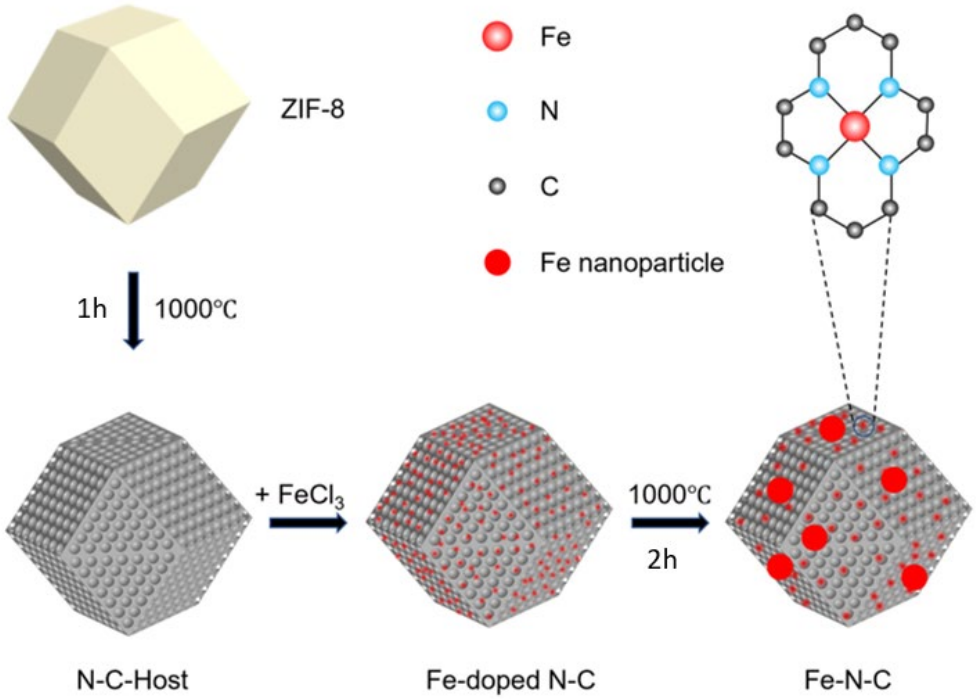

Fig. S1 Schematic illustration for the synthesis of Fe-N-C catalyst.

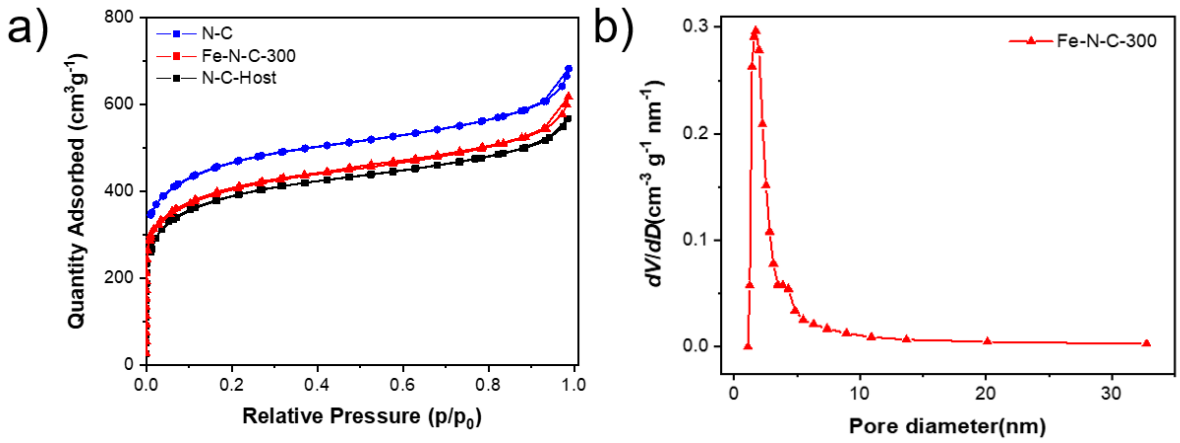

Fig. S2. (a) N_2 adsorption and desorption isotherms of N-C host, N-C, and Fe-N-C-300. (b) pore size distribution of Fe-N-C-300.

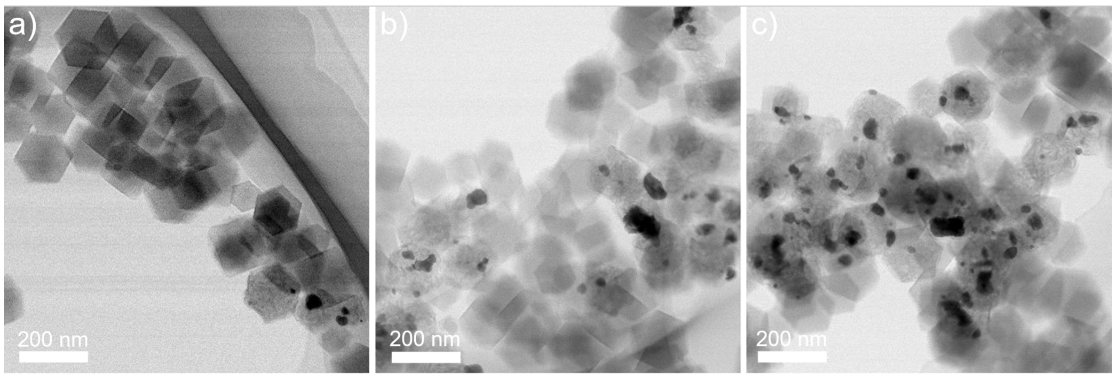

Fig. S3. TEM image of (a) Fe-N-C-100, (b) Fe-N-C-300, and (c) Fe-N-C-500.

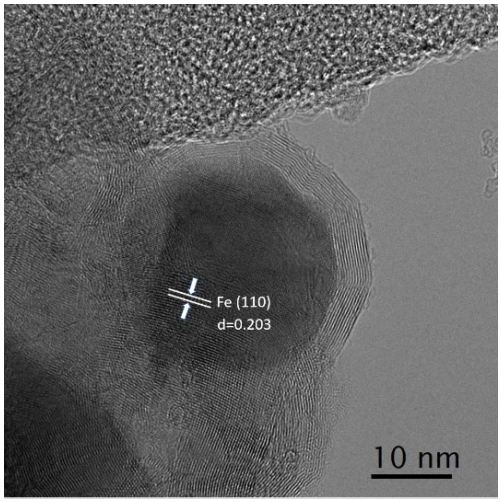

Fig. S4. TEM image of the Fe nanoparticles coated by graphitic carbon shell.

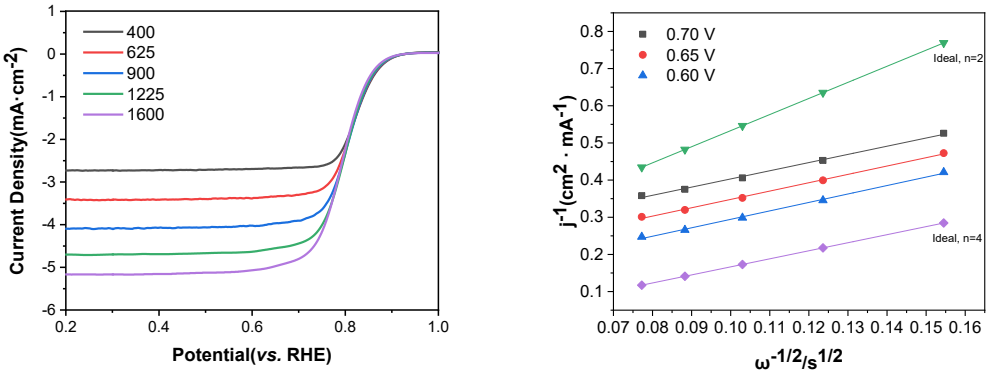

Fig. S5. LSV curve under different rotating speed and corresponding K-L analysis.

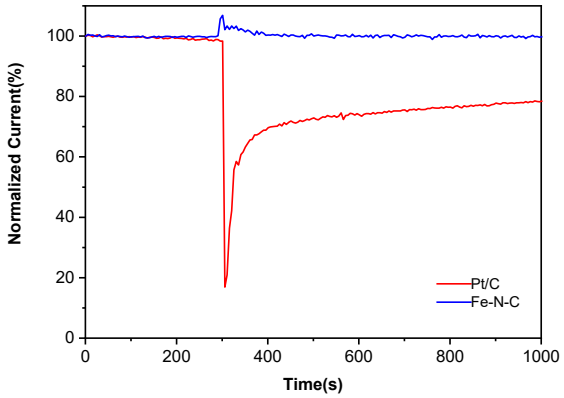

Fig. S6. The methanol tolerance evaluation by chronoamperometry at 0.5 V and adding 1 M methanol around 300 s.

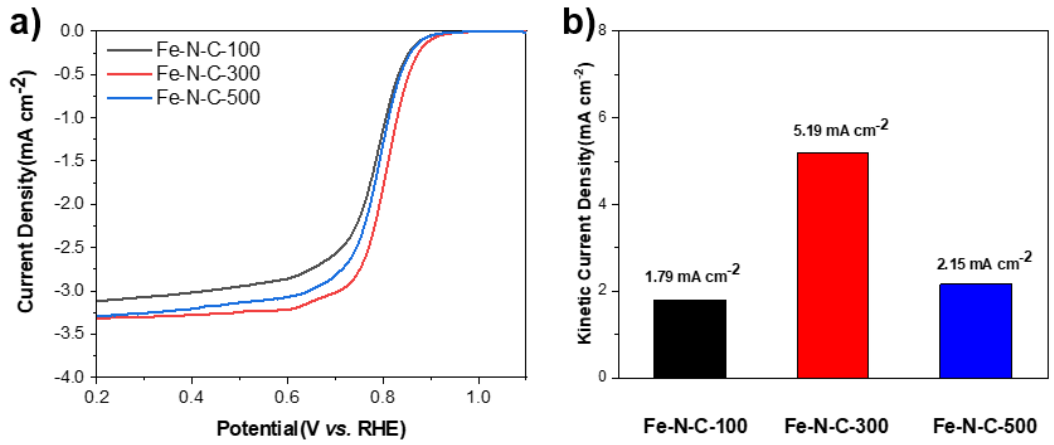

Fig. S7. a). LSV curve of indicated catalyst, $E_{1/2}$ of Fe-N-C-100/300/500 is 0.79, 0.81, and 0.79 V (*vs.* RHE), respectively. b). Kinetic current density of Fe-N-C-100/300/500 @ 0.8V.

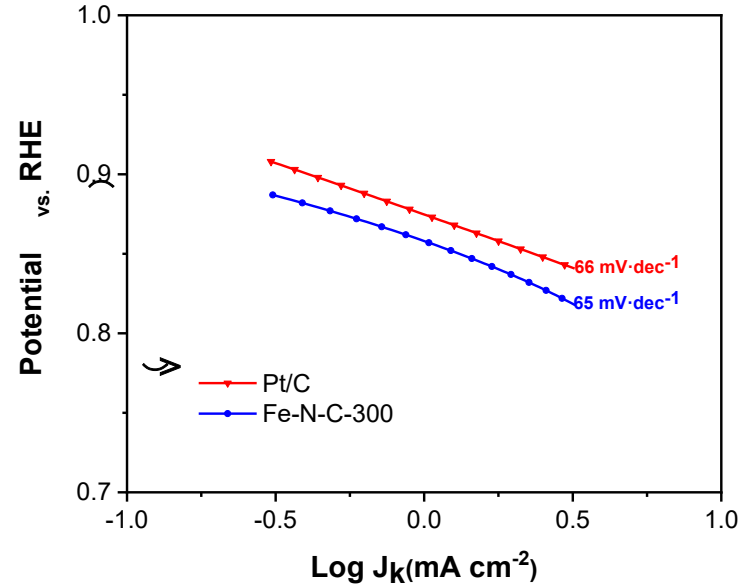

Fig. S8. Tafel plots of Fe-N-C-300 and Pt/C.

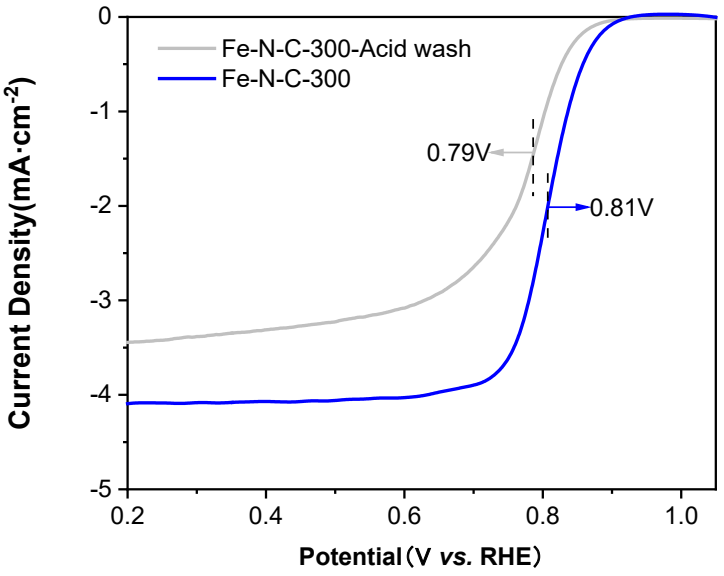

Fig. S9. LSV curve of Fe-N-C-300 before and after acid wash

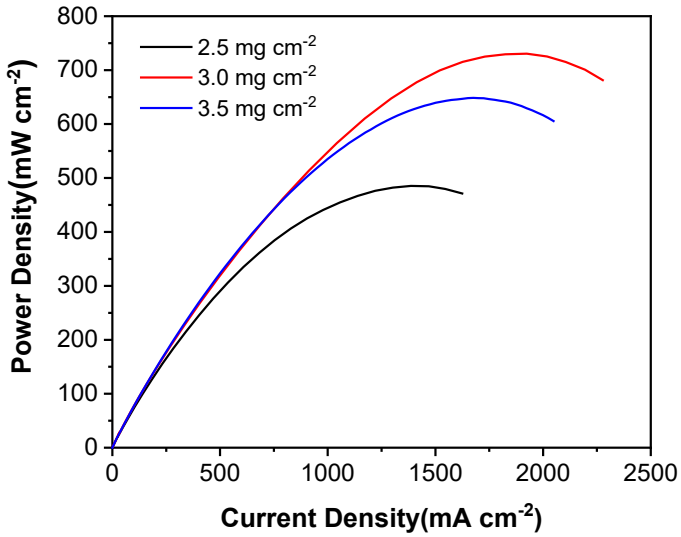

Figure S10. PEMFC power density curves of Fe-N-C-300 with the indicated cathode loadings (Testing conditions: 80 °C, 100 % humidified H_2 and O_2 with flow rate of 0.1 and 0.4 L·min^{-1}, respectively, back pressure is 1.0 bar on both anode and cathode side.)

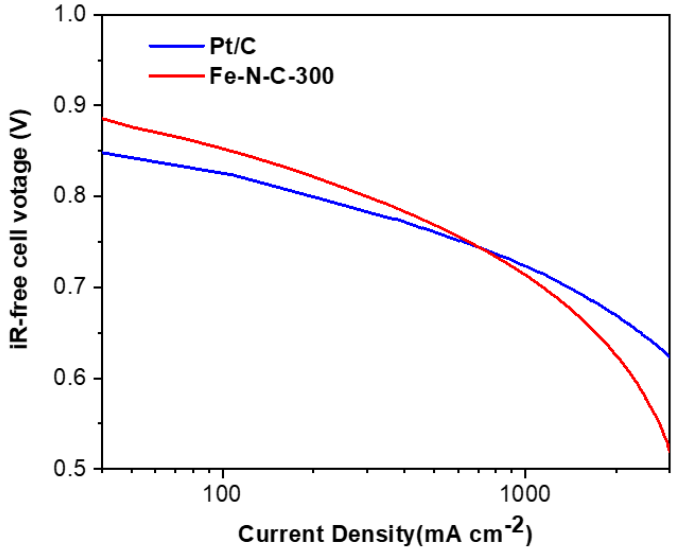

Fig. S 11. Tafel plots of the iR-free polarization curves for MEAs using Pt/C and Fe-N-C-300 as cathode.

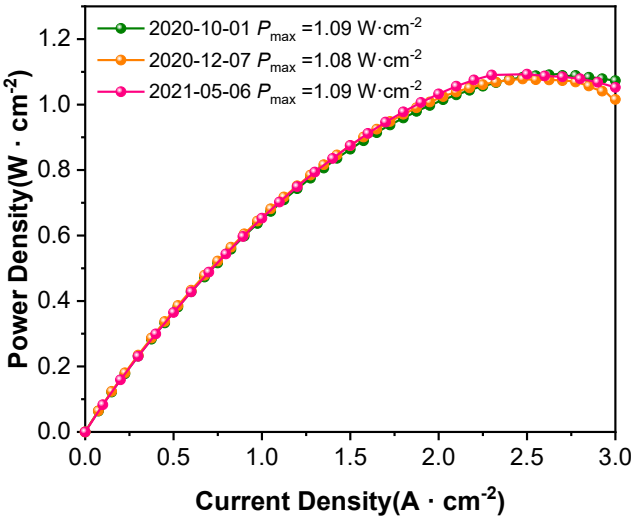

Figure S12. Repeated measurements of fuel cells.

Three independent fuel cell measurements with Fe-N-C-300 made in different batch as cathode catalysts demonstrate a good reproducibility. The results show an average peak power density of ~ 1.1 W cm^{-2}. Test conditions: cathode loading 3 mg cm^{-2}, 80 °C, 100% RH, 2.5 bar H_2-O_2.

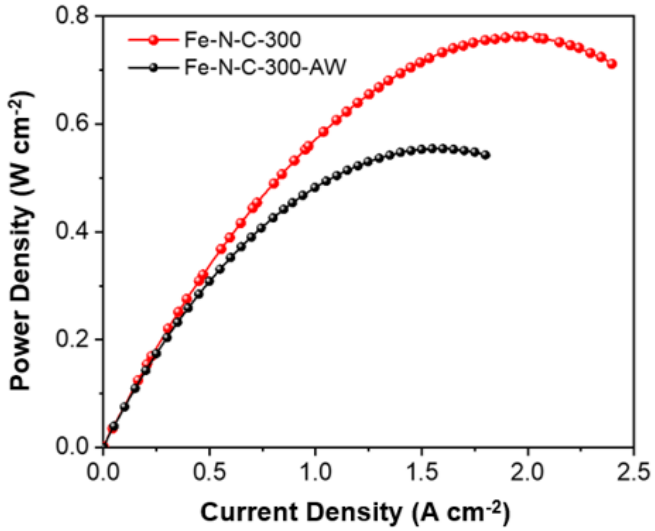

Figure S13. Power density curves of Fe-N-C-300 and Fe-N-C-300-AW under H_2-O_2, 1.0 bar.

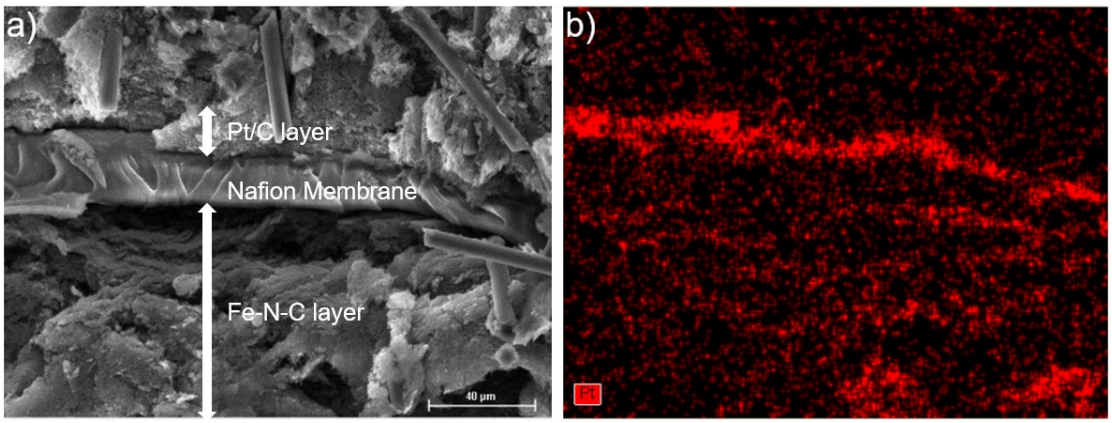

Fig. S14. a). Cross section SEM image of a MEA using Fe-N-C catalyst (loading of 3 $mg \cdot cm^{-2}$) as cathode and Pt/C (0.2 $mg_{Pt} \cdot cm^{-2}$)) as anode. (The layer in-between is the nafion membrane) **b).** Corresponding EDS image of Pt.

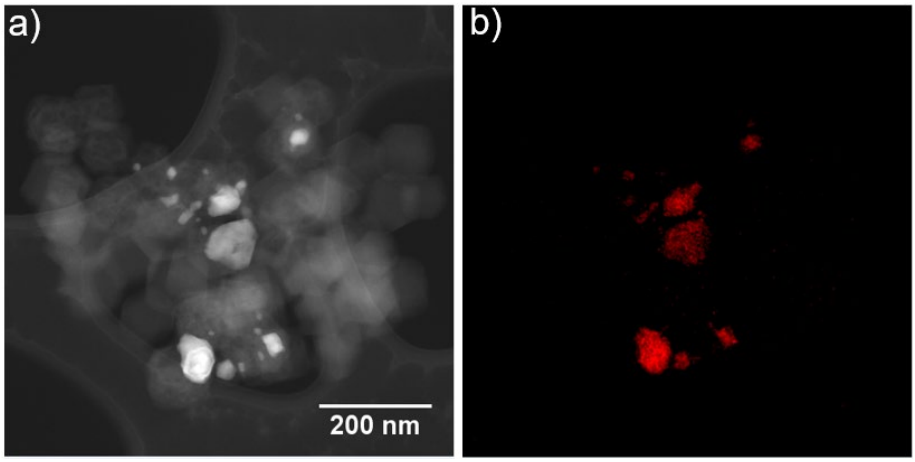

Fig. S15. SEM image of **a).** Fe-N-C-300 and **b).** Corresponding EDS mapping of Fe.

3. Supplemental Table

Table S1. BET surface area of indicated materials.

Sample	N-C-Host	Fe-doped N-C	N-C	Fe-N-C-300
BET surface area (m^2 g^{-1})	1282	1143	1522	1334

Table S2. C, N, O, and Fe contents in the Fe-N-C-100/300/500 determined by XPS measurements.

Sample	N-C	Fe-N-C-100	Fe-N-C-300	Fe-N-C-500
C 1s (at%)	78.51	82.88	83.37	85.23
N 1s (at%)	5.68	5.27	5.21	4.28
O 1s (at%)	4.98	8.84	8.42	7.43
Fe 2p (at%)	-	3.01	3.00	3.05
Zn 2p (at%)	10.84	-	-	-

Table S3. Fe contents in the catalyst obtained by ICP-OES measurements.

Sample	Fe(wt.%)
Fe-N-C-100	1.13
Fe-N-C-300	5.07
Fe-N-C-500	8.28
Fe-N-C-300-AW	1.07

Table S4. Comparison of ORR performance for Fe-N-C-300 with reported excellent performance Fe-based electrocatalysts in acid media.

Catalyst	$E_{1/2}$ (V *vs.* RHE)	Ref
Fe-N-C-300	**0.81**	**This work**
Fe-N-C-3	0.81	[2]
FeCo/C-800	0.76	[3]
Fe-ZIF	0.85	[4]
Fe-N-C-950	0.78	[5]
(CM+PANI)-Fe-C	0.80	[6]
FeSAs/PTF-600	0.77	[7]
FePhenMOF–ArNH3	0.78	[8]
SA-Fe-N nanosheets	0.80	[9]

Table S5. Fuel cell performance of previously reported Fe-N-C catalysts.

Catalyst	P_{max} under H_2-O_2	P_{max} under H_2-Air	Ref.
Fe-N-C-300	**1.08 W cm $^{-2}$**	**0.45 W cm $^{-2}$**	**This work**
(CM+PANI)-Fe-C	0.87 W cm $^{-2}$	0.42 W cm $^{-2}$	[6]
Fe-N-C-Phen-PANI	1.06 W cm $^{-2}$	0.38 W cm $^{-2}$	[10]
Fe SAs/N-C	0.75 W cm $^{-2}$	0.35 W cm $^{-2}$	[11]
1.5Fe-ZIF	0.67 W cm $^{-2}$	0.36 W cm $^{-2}$	[12]
C-FeHZ8@g-C3N4-950	0.63 W cm $^{-2}$	-	[13]
Fe-N/CNT-2	0.36 W cm $^{-2}$	-	[14]
ZIF-NC-0.5Fe-700	0.73 W cm $^{-2}$	0.32 W cm $^{-2}$	[15]
TPI@Z8(SiO2)-650-C	1.18 W cm $^{-2}$	0.42 W cm $^{-2}$	[16]

4. References：

1. Y. Li, X. Liu, L. Zheng, J. Shang, X. Wan, R. Hu, X. Guo, S. Hong and J. Shui, *Journal of Materials Chemistry A*, 2019, **7**, 26147-26153.
2. L. Gao, M. Xiao, Z. Jin, C. Liu, J. Ge and W. Xing, *Journal of Energy Chemistry*, 2019, **35**, 17-23.
3. Y. Chen, S. Ji, Y. Wang, J. Dong, W. Chen, Z. Li, R. Shen, L. Zheng, Z. Zhuang and D. Wang, *Angewandte Chemie*, 2017, **129**, 7041-7045.
4. H. Zhang, S. Hwang, M. Wang, Z. Feng, S. Karakalos, L. Luo, Z. Qiao, X. Xie, C. Wang and D. Su, *Journal of the American Chemical Society*, 2017, **139**, 14143-14149.
5. M. Xiao, J. Zhu, L. Ma, Z. Jin, J. Ge, X. Deng, Y. Hou, Q. He, J. Li and Q. Jia, *Acs Catalysis*, 2018, **8**, 2824-2832.
6. H. T. Chung, D. A. Cullen, D. Higgins, B. T. Sneed, E. F. Holby, K. L. More and P. Zelenay, *Science*, 2017, **357**, 479-484.
7. J.-D. Yi, R. Xu, Q. Wu, T. Zhang, K.-T. Zang, J. Luo, Y.-L. Liang, Y.-B. Huang and R. Cao, *ACS Energy Letters*, 2018, **3**, 883-889.
8. J. Li, S. Ghoshal, W. Liang, M.-T. Sougrati, F. Jaouen, B. Halevi, S. McKinney, G. McCool, C. Ma and X. Yuan, *Energy & Environmental Science*, 2016, **9**, 2418-2432.
9. Z. Miao, X. Wang, M. C. Tsai, Q. Jin, J. Liang, F. Ma, T. Wang, S. Zheng, B. J. Hwang and Y. Huang, *Advanced Energy Materials*, 2018, **8**, 1801226.
10. X. Fu, P. Zamani, J. Y. Choi, F. M. Hassan, G. Jiang, D. C. Higgins, Y. Zhang, M. A. Hoque and Z. Chen, *Advanced Materials*, 2017, **29**, 1604456.
11. Z. Yang, Y. Wang, M. Zhu, Z. Li, W. Chen, W. Wei, T. Yuan, Y. Qu, Q. Xu and C. Zhao, *ACS Catalysis*, 2019, **9**, 2158-2163.
12. H. Zhang, H. T. Chung, D. A. Cullen, S. Wagner, U. I. Kramm, K. L. More, P. Zelenay and G. Wu, *Energy & Environmental Science*, 2019, **12**, 2548-2558.
13. Y. Deng, B. Chi, X. Tian, Z. Cui, E. Liu, Q. Jia, W. Fan, G. Wang, D. Dang and M. Li, *Journal of Materials Chemistry A*, 2019, **7**, 5020-5030.
14. D. Xia, X. Yang, L. Xie, Y. Wei, W. Jiang, M. Dou, X. Li, J. Li, L. Gan and F. Kang, *Advanced Functional Materials*, 2019, **29**, 1906174.
15. J. Li, H. Zhang, W. Samarakoon, W. Shan, D. A. Cullen, S. Karakalos, M. Chen, D. Gu, K. L. More and G. Wang, *Angewandte Chemie*, 2019, **131**, 19147-19156.
16. X. Wan, X. Liu, Y. Li, R. Yu, L. Zheng, W. Yan, H. Wang, M. Xu and J. Shui, *Nature Catalysis*, 2019, **2**, 259-268.